Bioorganic Chemistry 90 (2019) 103084

Contents lists available at ScienceDirect

Bioorganic Chemistry

journal homepage: www.elsevier.com/locate/bioorg

Search for multifunctional agents against Alzheimer's disease among non-imidazole histamine H3 receptor ligands. *In vitro* and *in vivo* pharmacological evaluation and computational studies of piperazine derivatives

Jakub Jończyk[a], Krzysztof Lodarski[a], Marek Staszewski[b], Justyna Godyń[a], Paula Zaręba[a], Ondrej Soukup[c,d], Jana Janockova[c], Jan Korabecny[c,d], Kinga Sałat[e], Natalia Malikowska-Racia[e], Michalina Hebda[a], Natalia Szałaj[a], Barbara Filipek[e], Krzysztof Walczyński[b], Barbara Malawska[a], Marek Bajda[a,*]

[a] Department of Physicochemical Drug Analysis, Faculty of Pharmacy, Jagiellonian University Medical College, Medyczna 9, 30–688 Kraków, Poland
[b] Department of Synthesis and Technology of Drugs, Medical University of Łódź, Muszyńskiego 1, 90–145 Łódź, Poland
[c] Biomedical Research Center, University Hospital Hradec Kralove, Sokolska 581, 500 05 Hradec Kralove, Czech Republic
[d] National Institute of Mental Health, Topolova 748, 250 67 Klecany, Czech Republic
[e] Department of Pharmacodynamics, Jagiellonian University Medical College, Medyczna 9, 30–688 Kraków, Poland

ARTICLE INFO

Keywords:
Multi-target-directed ligands
Alzheimer's disease
H3 histamine receptor
Cholinesterase inhibitors
Acetylcholinesterase
Butyrylcholinesterase
Thiazole
Piperazine

ABSTRACT

In the search for new treatments for complex disorders such as Alzheimer's disease the Multi-Target-Directed Ligands represent a very promising approach. The aim of the present study was to identify multifunctional compounds among several series of non-imidazole histamine H3 receptor ligands, derivatives of 1-[2-thiazol-5-yl-(2-aminoethyl)]-4-*n*-propylpiperazine, 1-[2-thiazol-4-yl-(2-aminoethyl)]-4-*n*-propylpiperazine and 1-phenoxyalkyl-4-(amino)alkylopiperazine using *in vitro* and *in vivo* pharmacological evaluation and computational studies. Performed *in vitro* assays showed moderate potency of tested compounds against acetylcholinesterase (AChE) and butyrylcholinesterase (BuChE). Molecular modeling studies have revealed possible interactions between the active compounds and both AChE and BuChE as well as the human H3 histamine receptor. Computational studies showed the high drug-likeness of selected compounds with very good physicochemical profiles. The parallel artificial membrane permeation assay proved outstanding blood–brain barrier penetration in test conditions. The most promising compound, **A12**, chemically methyl(4-phenylbutyl){2-[2-(4-propylpiperazin-1-yl)-1,3-thiazol-5-yl]ethyl}amine, possesses good balanced multifunctional profile with potency toward studied targets - H3 antagonist activity (pA_2 = 8.27), inhibitory activity against both AChE (IC_{50} = 13.96 μM), and BuChE (IC_{50} = 14.62 μM). The *in vivo* pharmacological studies revealed the anti-amnestic properties of compound **A12** in the passive avoidance test on mice.

1. Introduction

Alzheimer's disease (AD) is an irreversible, progressive neurodegenerative brain disorder leading to pronounced cognitive deficits, such as disorientation, and impairments in learning and memory functions. The pathophysiology of the disease includes deficiency in cholinergic neurotransmission, dysfunctions in the release of other neuro-signaling substances (including glutamatergic, adrenergic, serotonergic,

Abbreviations: ACh, acetylcholine; AChE, acetylcholinesterase; AD, Alzheimer's disease; BBB, blood–brain barrier; BuChE, butyrylcholinesterase; CA, alpha carbon; ChEI, cholinesterase inhibitor; CI, confidence interval; CNS, central nervous system; *cp*, *cavia porcellus*, guinea pig; DMSO, dimethyl sulfoxide; DTNB, 5,5′-dithiobis-(2-nitrobenzoic acid); *ee*, *electrophorus electricus*, electric eel; *eq*, *equus ferus caballus*, horse; H3R, histamine H3 receptor; *hs*, *homo sapiens*, human; I.R., infrared; K_m, michaelis constant; MTDL, multi-target-directed ligands; *n.a.*, non-active; *n.d.*, non-determined; *n.s.*, non-soluble; PA, passive avoidance; PAMPA, parallel artificial membrane permeability assay; PAS, peripheral anionic site; PBL, polar brain lipid; PBS, phosphate-buffered saline; *rn*, *rattus norvegicus*, rat; SD, standard deviation; SEM, standard error of the mean; SP, standard precision; TM, transmembrane; V_{max}, the maximum reaction velocity

* Corresponding author.
E-mail address: marek.bajda@uj.edu.pl (M. Bajda).

https://doi.org/10.1016/j.bioorg.2019.103084
Received 11 February 2019; Received in revised form 24 May 2019; Accepted 24 June 2019
Available online 26 June 2019
0045-2068/ © 2019 Elsevier Inc. All rights reserved.

dopaminergic, histaminergic substances), changes in β-amyloid protein metabolism resulting in the formation of neurotoxic senile plaques, tau protein aggregation, progression of inflammation and damage caused by oxidative stress [1,2]. AD is a complex disease with a multifaceted pathomechanism, which, despite significant progress in the field, remains unclear. Considering this intertwined etiology, the classic 'single target molecule' approach may not be sufficiently effective to address AD. In recent years, the development of Multi-Target-Directed Ligands (MTDLs) has been intensively used as a more promising strategy, giving the chance to develop effective treatment of the disease [3,4]. Ligands interacting with multiple targets can work in a complementary or additive manner. In the first approach, a compound that interacts with two or more targets can act at different levels of pathogenic changes. The additive mode of the multifunctional action of the ligand is observed when the interaction on both targets leads to a similar, coherent effect [5–8]. Considering that both the histamine H3 receptor (H3R) and acetylcholinesterase (AChE) are involved in the regulation of the amount of central neurotransmitters, a combination of these effects can produce very beneficial effects [9,10].

According to the cholinergic hypothesis, which is one of the oldest and most extensively studied theories regarding AD pathogenesis, symptoms of the AD are caused by a decline in the number of cholinergic neurons [11]. The majority of therapeutics approved for AD belong to the class of AChE inhibitors [12]. Inhibition of this enzyme increases the amount of acetylcholine (ACh) in the synaptic cleft which leads to significant relief in AD symptoms [13]. Inhibition of AChE and BuChE are still the subject of intensive research in the field of medical chemistry [14,15]. Involvement of histamine H3 receptors (H3R) in the cognitive process has been confirmed since blocking the central H3R receptor proved induction of the release of procognitive neurotransmitters, *i.a.* acetylcholine [16]. Some antagonists of H3R, for example thioperamide and pitolisant (Fig. 1) have shown improvement in multiple aspects of memory processing during passive avoidance tests on rodents [9,17]. Other selective and potent H3R antagonists, *i.e.* GSK-239512 and MK-3134, after proving their procognitive activity in a variety of animal models, were subject of clinical trials. During study on patients with mild-to-moderate Alzheimer's disease GSK239512 improved episodic memory but no statistically significant changes were observed on other cognitive domains measured with Assessment Scale–Cognitive Subscale (ADASCog) [18]. The effect of MK-3134 alone and in combination with acetylcholinesterase inhibitor - donepezil on the cognitive impairment associated with scopolamine was tested on healthy volunteers. Results assessed with the Groton Maze Learning Task (GMLT) provided evidence for cognitive improvement through MK-3134 and demonstrated that the combination of MK-3134 and donepezil suppressed the negative effect of scopolamine to a greater extent than either drug alone [19]. It is worthy to add that pitolisant has been approved currently for the treatment of narcolepsy, and also is still under studies for potential treatment various cognitive and sleep disorders [20].

Several research groups have developed multifunctional ligands connecting H3R antagonists and cholinesterase inhibitors (ChEIs) with interesting results [9,17,24–26]. Structures of selected ChEIs and histamine H3 receptor antagonists/inverse agonists are presented in Fig. 2. These compounds possess various activities toward both targets; the most promising seems to be the **CHEMBL3323053** compound with well-balanced potencies and *in vivo* procognitive properties [9,17,24–26]. These dual acting compounds have been designed by linking or merging structurally active fragments interacting with AChE and histamine H3 receptors. Another way to search for dual AChE inhibitors and H3R antagonists is screening of known H3R ligands toward inhibitory potency against cholinesterase [27–29]. The presented research applied the latter strategy. This approach is resemble to repurposing drug discovery strategy, by searching new possible therapeutic indication for existing drugs on the market [30–32].

Our research focuses on novel cholinesterase inhibitors with additional properties as potential multifunctional anti-Alzheimer's agents [33–35]. Herein, we describe the pharmacological evaluation and molecular modeling of several series of non-imidazole histamine H3 receptor ligands, derivatives of thiazol and piperazine [21,36–38]. The target compounds were previously designed and synthesized as histamine H3 receptor ligands with proved *in vitro* antagonist potency. The main goal of the presented research was the discovery of multifunctional ligands that can be used against AD.

The pharmacological studies included *in vitro* assays for AChE and butyrylcholinesterase (BuChE) inhibition, and blood–brain barrier (BBB) permeability using the parallel artificial membrane permeability assay (PAMPA), and *in vivo* assessment of the impact on memory in mice. The molecular modeling included docking into both cholinesterases and studies of interactions with the homology model of histamine H3 receptors. The computational studies included estimation of the physicochemical properties of tested compounds.

2. Results and discussion

2.1. Biological screening

We conducted biological screening involving enzymatic assays against AChE and BuChE for 50 non-imidazole histamine H3 receptor antagonists. The spectrophotometric Ellman's assay was applied to determine the cholinesterase inhibition profiles of the test compounds [39]. In Ellman's assay, AChE from electric eel (*ee*AChE) and BuChE from horse serum (*eq*BuChE) were used. The results were compared to those of reference compounds, *i.e.*, cholinesterase inhibitors – tacrine, donepezil and galantamine, as well as a histamine H3 ligand – pitolisant. The tested compounds can be assigned to one of three chemical groups:

- derivatives of 1-[2-thiazol-5-yl-(2-aminoethyl)]-4-*n*-propylpiperazine – Series **A**
- derivatives of 1-[2-thiazol-4-yl-(2-aminoethyl)]-4-*n*-propylpiperazine – Series **B**
- derivatives of 1-phenoxyalkyl-4-(amino)alkylopiperazine – Series **C**

The chemical structures of the compounds belonging to the library of H3 antagonists, together with obtained results, are shown in Tables

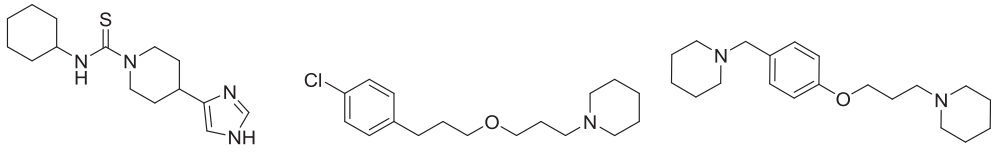

Thioperamide
cp pA_2 = 8.47

Pitolisant
cp pA_2 = 8.3

JNJ-5207852
rn pA_2 = 8.94

Fig. 1. Structures of selected histamine H3 receptor antagonists/inverse agonists with pA_2 values against guinea pig (*cp*) for Thiperamide [21] and Pitolisant [22] and rat (*rn*) H3 receptors, JNJ5207852 [23].

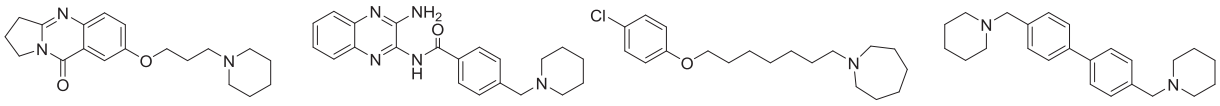

CHEMBL3323053
hs H3R *Ki* = 2.54μM
hs AChE IC50 = 5.4 μM
eq BuChE IC50 = 122.3 μM

CHEMBL1929400
hs H3R IC50 = 0.28μM
ee AChE IC50 = 0.483 μM

CHEMBL3747910
hs H3R *Ki* = 0.203μM
ee AChE IC50 = 1.93 μM
eq BuChE IC50 = 1.64 μM

CHEMBL380101
hs H3R *Ki* = 0.3 nM
rn AChE IC50 = 5.89 μM

Fig. 2. Examples of Multi-Target-Directed Ligands; CHEMBL3323053 [9,24], CHEMBL1929400 [26], CHEMBL3747910 [25] and CHEMBL380101 [17] combining activity against human (*hs*) H3R and cholinesterases from rat (*rn*), horse serum (*eq*) or electric eel (*ee*).

1–3. In order to facilitate the comparison of corresponding derivatives from A and B series, the complementary numbering was assigned to them.

During the first step, the percentage of enzyme inhibition was measured using a 50 μM screening concentration of the tested compounds. The IC_{50} values were experimentally determined for the most potent inhibitors revealed during the screening. Based on these results, we found that the compounds from series A – C compared to the reference drugs presented a moderate to weak ability to inhibit cholinesterases. Among series A and B, derivative **A13** with an IC_{50} equal to 4.45 μM was the most active AChE inhibitor. Compound **B14** with an estimated IC_{50} equal to 5.75 μM was the strongest inhibitor of BuChE among the compounds from series A and B. Derivatives in the subset C were generally inactive against AChE. Nevertheless, **C20** proved to be the most active inhibitor of BuChE of all the tested compounds. The IC_{50} value of **C20** was equal to 3.27 μM.

Looking at the results of screening, we observed a clear relationship between the ligand structure and activity toward cholinesterases. In all thiazole derivatives, activity against cholinesterases was associated with the presence of the phenylalkyl fragment in the ethylamine

Table 1
Chemical structures of 1-[2-thiazol-5-yl-(2-aminoethyl)]-4-*n*-propylpiperazine derivatives (series A). Inhibitory activity on *ee*AChE, *eq*BuChE, and *cp*H3 antagonistic activity.

Series A

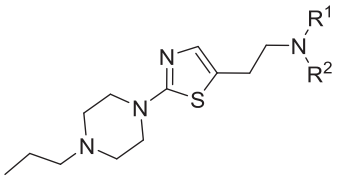

Cpd.	R^1	R^2	*ee*AChE		*eq*BuChE		*cp*H_3
			% I[a]	IC_{50} [μM][b]	% I[a]	IC_{50} [μM][b]	pA_2[c]
A1	−H	−H	13.58 ± 2.40	*n.d.*	5.08 ± 3.50	*n.d.*	7.19
A4	$-CH_3$	$-C_3H_7$	62.33 ± 1.27	*n.d.*	44.65 ± 6.03	*n.d.*	7.53
A5	$-CH_3$	$-C_5H_{11}$	68.94 ± 1.26	*n.d.*	41.93 ± 2.42	*n.d.*	7.05
A6	−H	−CHO	34.24 ± 1.39	*n.d.*	4.60 ± 4.37	*n.d.*	6.93
A7	$-CH_3$	−CHO	19.39 ± 1.48	*n.d.*	11.89 ± 2.49	*n.d.*	7.26
A9	$-CH_3$	$-COCH_2CH_3$	31.86 ± 1.38	*n.d.*	22.12 ± 3.65	*n.d.*	7.36
A11	$-CH_3$	$-(CH_2)_2C_6H_5$	82.12 ± 1.15	**15.57** (12.56–19.29)	64.00 ± 1.87	**52.35** (38.45–71.27)	7.61
A12	$-CH_3$	$-(CH_2)_3C_6H_5$	78.24 ± 0.19	**13.96** (13.06–14.62)	79.12 ± 1.05	**14.62** (11.92–20.15)	8.27
A13	$-CH_3$	$-(CH_2)_4C_6H_5$	93.27 ± 0.47	**4.45** (3.72–5.33)	74.38 ± 0.88	**29.62** (24.09–36.43)	7.80
A14	$-CH_3$	$-(CH_2)_5C_6H_5$	79.86 ± 0.43	**23.58** (20.72–26.83)	84.51 ± 0.62	**13.87** (12.83–14.98)	7.25
A15	$-CH_3$	$-COC_6H_5$	53.39 ± 0.79	*n.d.*	40.84 ± 4.48	*n.d.*	7.45
A16	$-CH_3$	$-COC_6H_4CH_3$(p)	55.34 ± 0.27	*n.d.*	51.70 ± 2.69	*n.d.*	7.61
A17	$-CH_3$	$-COC_6H_4NO_2$(p)	45.71 ± 2.06	*n.d.*	20.26 ± 4.85	*n.d.*	7.76
A18	$-CH_3$	$-COC_6H_4Cl$(p)	39.11 ± 2.97	*n.d.*	51.33 ± 1.98	*n.d.*	7.73
Tacrine HCl			*n.d.*	0.021 (0.016–0.028)	*n.d.*	0.003 (0.003–0.004)	*n.d.*
Donepezil HCl			*n.d.*	0.012 (0.009–0.016)	*n.d.*	1.83 (1.41–2.37)	*n.d.*
Galantamine HBr			*n.d.*	0.380 (0.290–0.510)	*n.a.*	*n.d.*	*n.d.*
Pitolisant $(COOH)_2$			3.04 ± 0.97[d]	*n.d.*	56.29 ± 0.15 [d]	8.42 (8.25–8.6)	8.3 [e]

n.a. – non-active at screening concentration.
n.d. – non-determined.
[a] Inhibition percentage of enzyme at 50 μM concentration. Values are expressed as means ± standard deviation (SD) for at least three independent experiments.
[b] IC_{50} inhibitory concentration of enzyme. Values are expressed as means with confidence interval (CI) for at least three experiments.
[c] pA_2 value obtained from *in vitro* test system on the guinea pig jejunum [21,36–38].
[d] Inhibition percentage of enzyme at 10 μM concentration. Values are expressed as means ± SD for at least three independent experiments.
[e] pA_2 value according to Liedtke et al. [22].

Table 2
Chemical structures of 1-[2-thiazol-4-yl-(2-aminoethyl)]-4-*n*-propylpiperazine of derivatives (series B). Inhibitory activity on *ee*AChE, *eq*BuChE, and *cp*H3 antagonistic activity.

Series B

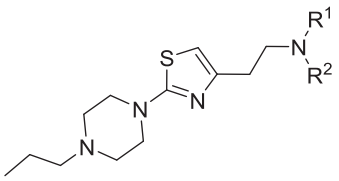

Cpd.	R^1	R^2	*ee*AChE		*eq*BuChE		*cp*H_3
			% I[a]	IC_{50} [μM][b]	% I[a]	IC_{50} [μM][b]	pA_2[c]
B1	−H	−H	7.30 ± 4.76	*n.d.*	*n.a.*	*n.d.*	*n.d.*
B2	$-CH_3$	−H	25.85 ± 7.10	*n.d.*	23.39 ± 6.89	*n.d.*	*n.d.*
B3	$-CH_3$	$-CH_3$	25.00 ± 0.88	*n.d.*	16.19 ± 3.82	*n.d.*	6.76
B4	$-CH_3$	$-C_3H_7$	40.48 ± 0.56	*n.d.*	29.49 ± 1.87	*n.d.*	6.92
B8	$-CH_3$	$-COCH_3$	9.80 ± 2.69	*n.d.*	13.27 ± 1.68	*n.d.*	*n.d*
B10	$-CH_3$	$-CH_2C_6H_5$	68.13 ± 0.93	**18.25** (15.60–21.35)	62.82 ± 3.39	**23.74** (19.35–29.12)	7.12
B11	$-CH_3$	$-(CH_2)_2C_6H_5$	63.85 ± 2.43	**25.54** (22.30–29.26)	70.90 ± 0.95	**17.51** (15.20–20.18)	6.81
B12	$-CH_3$	$-(CH_2)_3C_6H_5$	82.48 ± 1.55	**8.52** (7.05–10.30)	79.31 ± 1.47	**8.72** (7.11–10.70)	6.61
B13	$-CH_3$	$-(CH_2)_4C_6H_5$	70.87 ± 3.06	**18.34** (15.78–21.32)	83.23 ± 2.05	**5.98** (5.38–6.64)	6.72
B14	$-CH_3$	$-(CH_2)_5C_6H_5$	60.78 ± 2.65	**31.61** (27.52–36.30)	89.47 ± 0.95	**5.75** (4.90–6.74)	6.69
B15	$-CH_3$	$-COC_6H_5$	12.63 ± 5.32	*n.d.*	25.07 ± 1.69	*n.d.*	5.65
B16	$-CH_3$	$-COC_6H_4CH_3$(p)	30.54 ± 8.76	*n.d.*	30.17 ± 0.95	*n.d.*	5.80
B17	$-CH_3$	$-COC_6H_4NO_2$(p)	29.56 ± 6.06	*n.d.*	20.46 ± 0.31	*n.d.*	6.03

n.a. – non-active at screening concentration.
n.d. – non-determined.
[a] Inhibition percentage of enzyme at 50 μM concentration. Values are expressed as means ± SD for at least three independent experiments.
[b] IC_{50} inhibitory concentration of enzyme. Values are expressed as means with confidence interval (CI) for at least three experiments.
[c] pA_2 value obtained from *in vitro* test system on the guinea pig jejunum [21,36–38].

substituent. Comparing analogs from series A and B, it can be seen that the derivatives from series A are generally more active against AChE than their 2,4-substituted analogs (series B). Similarly, derivatives of series B are significantly more active against BuChE than their counterparts in family A. Specific differences in activity are presented in Fig. 3.

These results show that the position of the ethylamine substituent in the thiazole ring has a significant effect on the selectivity of ligands between cholinesterases. The difference in the substitution of the thiazole ring also detracts from the antagonist activity of histamine H3 receptors. It is worth noting that 2,5-substituted derivatives are stronger inhibitors of AChE and are also more potent H3-receptor antagonists (Fig. 4).

Ligands assigned to series C are *ω*-phenoxyalkyl derivatives of amino alkyl piperazine. Biological screening proved that compounds from series C are generally stronger inhibitors of BuChE than AChE. The highest recorded AChE activity among the examined compounds can be assigned to derivative **C8**, with an IC_{50} equal to 13.53 μM. The most potent BuChE inhibitory properties among derivatives of series C, with IC_{50} values of the level of single μM, were displayed by derivatives **C18** and **C20**. The IC_{50} values determined for these compounds are 6.24 μM and 3.27 μM, respectively. The clearly marked relationship between the structure and activity of the tested compounds indicates that the BuChE inhibitory activity in series C (**C9–C13**) increases with the elongation of the alkyl linker between the basic centers, reaching its highest value for derivatives with a heptyl linker (**C13**). On the other hand, based on the comparison of compounds **C14–C17**, we can further suggest the longer the alkyl chain attached to the free amino group is present, the lower BuChE the inhibition occurs. Due to the low solubility of derivatives **C8**, **C10**, **C19**, **C21** and **C22** from series C, determination of reliable IC_{50} values against cholinesterases was impossible. The obtained results allowed us to choose the most promising dual acting compounds for further *in vitro/in vivo* studies.

2.2. Kinetic study of AChE and BuChE inhibition

For kinetic studies we selected compounds **A12**, **A13** and **C20** as the most potent ChE inhibitors from the tested series. Analysis of the Lineweaver-Burk (L-B) (Fig. 5A–D) and Cornish-Bowden (Supporting Information) reciprocal plots for both *ee*AChE and *eq*BuChE with calculated V_{max} (the maximal reaction velocity) and K_m (Michaelis constant) values showed that all three compounds display a mixed type of enzyme inhibition. The L-B reciprocal plots for **A12** (Fig. 5A and B) were inconclusive; however, analysis of Cornish-Bowden plots and calculated Km values confirmed a mixed type of inhibition for both enzymes. On the **A13** L-B reciprocal plot, we observed increased slopes (decreased V_{max}) and decreased intercepts (lower K_m) at increasing concentrations of the inhibitor (Fig. 5C). For **C20**, the L-B reciprocal plot showed increased slopes (decreased V_{max}) and increased intercepts (higher Km) at increasing concentrations of the inhibitor (Fig. 5D). A mixed type of enzyme inhibition indicates that the test compounds may interact with both catalytic active sites and peripheral anionic sites of cholinesterase at the same time [40].

2.3. Molecular modeling

2.3.1. Docking studies on AChE and BuChE

The tested compounds were docked into the AChE crystal structure from *Torpedo californica* in complex with donepezil (PDB: 1EVE), as well as into the crystal structure of human butyrylcholinesterase (PDB:

Table 3
Chemical structures of 1-phenoxyalkyl-4-(amino)-alkylopiperazine derivatives (series C). Inhibitory activity toward *ee*AChE, *eq*BuChE, and *cp*H3 antagonistic activity.

Series C

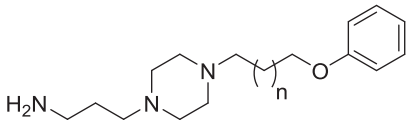

Cpd.	n	eeAChE		eqBuChE		cpH_3
		% I[a]	IC_{50} [μM][b]	% I[a]	IC_{50} [μM][b]	pA_2[c]
C1	0	n.a.	*n.d.*	n.a.	*n.d.*	6.75
C2	1	9.80 ± 1.91	*n.d.*	2.34 ± 8.13	*n.d.*	6.29
C3	2	5.06 ± 1.55	*n.d.*	8.06 ± 6.01	*n.d.*	6.62
C4	3	8.20 ± 4.15	*n.d.*	10.14 ± 4.64	*n.d.*	6.80
C5	4	21.37 ± 18.9	*n.d.*	21.61 ± 13.7	*n.d.*	6.72
C6	5	40.02 ± 0.82	*n.d.*	55.86 ± 3.33	**29.99** (22.07–40.75)	7.04
C7	6	54.74 ± 7.07	**39.13** (32.06–47.76)	38.03 ± 3.05	*n.d.*	6.84
C8	7	74.77 ± 1.16	**13.53** (11.64–15.73)	57.02 ± 0.65	*n.s*	6.99

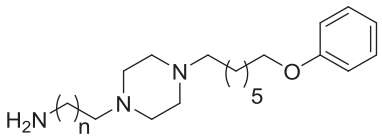

Cpd.	n	eeAChE		eqBuChE		cpH_3
		% I[a]	IC_{50} [μM][b]	% I[a]	IC_{50} [μM][b]	pA_2[c]
C9	1	33.53 ± 2.03	*n.d.*	44.90 ± 3.55	*n.d.*	6.42
C10	3	41.14 ± 2.36	*n.d.*	59.44 ± 2.88	*n.s.*	7.18
C11	4	27.85 ± 2.81	*n.d.*	62.56 ± 2.49	**27.40** (23.85–31.49)	6.99
C12	5	20.71 ± 4.61	*n.d.*	61.89 ± 1.61	**21.97** (17.92–26.94)	6.67
C13	6	28.04 ± 3.03	*n.d.*	73.93 ± 0.72	**13.95** (11.54–16.86)	6.67

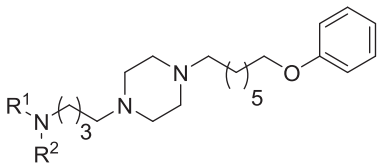

Cpd.	R^1	R^2	eeAChE		eqBuChE		cpH_3
			% I[a]	IC_{50} [μM][b]	% I[a]	IC_{50} [μM][b]	pA_2[c]
C14	$-CH_3$	$-CH_3$	48.44 ± 1.23	*n.d.*	86.93 ± 1.85	**10.86** (8.38–14.07)	7.01
C15	$-CH_3$	$-C_2H_5$	45.00 ± 1.94	*n.d.*	68.50 ± 0.90	**28.11** (25.15–31.42)	7.27
C16	$-CH_3$	$-C_3H_7$	29.42 ± 2.13	*n.d.*	58.17 ± 0.86	**28.84** (22.57–36.86)	7.05
C17	$-CH_3$	$-C_5H_{11}$	10.12 ± 1.99	*n.d.*	54.93 ± 0.97	**39.68** (32.96–47.77)	6.60
C18	$-CH_3$	$-CH_2-C_6H_5$	40.97 ± 1.88	*n.d.*	85.02 ± 0.47	**6.24** (5.32–7.33)	7.13
C19	$-CH_3$	$-C_3H_6-C_6H_5$	62.76 ± 1.83	*n.s.*	89.86 ± 0.23	*n.s*	7.04
C20	$-CH_3$	$-C_5H_{10}-C_6H_5$	64.27 ± 3.62	*n.s.*	92.74 ± 0.27	**3.27** (2.75–3.88)	6.95
C21	$-CH_3$	$-CO-C_6H_5$	12.83 ± 4.05	*n.d.*	82.09 ± 0.92	*n.s*	6.98
C22	$-CH_3$	$-CO-CF_3$	34.90 ± 11.1	*n.d.*	60.65 ± 4.71	*n.s*	7.00
C23	$-H$		50.80 ± 1.28	**48.64** (42.09–56.22)	78.05 ± 1.28	**11.34** (9.03–14.24)	7.12

n.d. – non-determined.
n.s. – non-soluble in test conditions.
[a] Inhibition percentage of enzyme at 50 μM concentration. Values are expressed as means ± SD for at least three independent experiments.
[b] IC_{50} inhibitory concentration of enzyme. Values are expressed as means with confidence interval (CI) for at least three experiments.
[c] pA_2 value obtained from *in vitro* test system on the guinea pig jejunum [21,36–38].

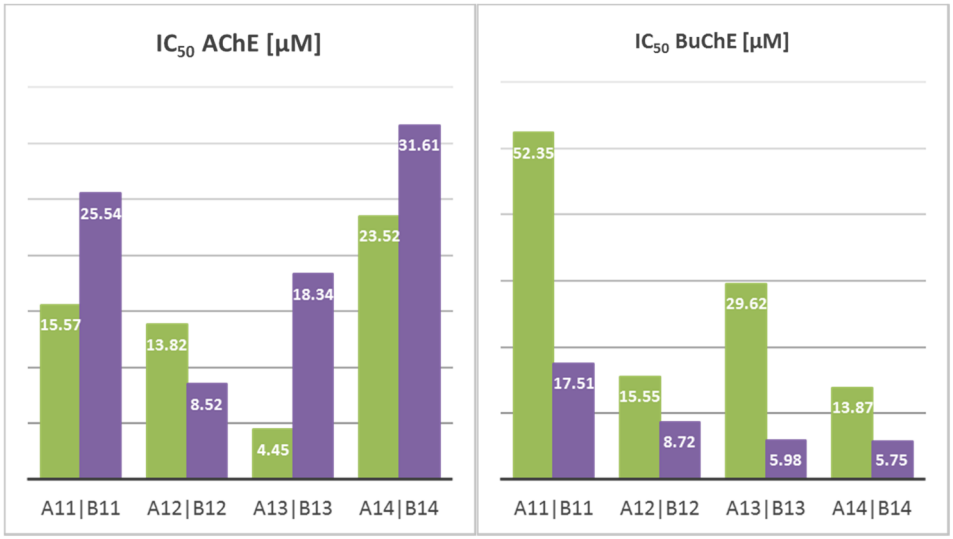

Fig. 3. Comparison of the IC_{50} values for AChE, BuChE inhibition for selected analogs from series A (green) and B (violet).

1P0I), to find the possible binding mode and to explain the reasons for varied potencies against cholinesterases. We used previously developed and validated methods for docking to both cholinesterases [41]. In the case of AChE, all active derivatives were arranged along the active gorge and blocked both catalytic and peripheral active sites. The predominance of phenylalkyl derivatives over other tested ligands in series A and B reported during bioassays correlated well with our *in silico* results. Compounds **A11–A14** and **B11–B14** established a very coherent binding mode in docking experiments. The most active AChE inhibitor, **A13**, is shown in Fig. 6 as an example of the final docking pose of phenylalkyl derivatives. The *N*-methyl-*N*-3-phenylalkyl fragment interacts with the anion binding site via TRP 84 (π–π) and PHE 330 (cation–π). The thiazole ring is located at the entrance to the active site creating aromatic interactions with PHE 290, PHE 331 and TYR 334. The hydrogen bond between preserved the water molecule (HOH 1254) and nitrogen from the thiazole ring deserves additional attention because of its presence, particularly in terms of the results of the docking of the most active derivatives from the A series. The length of the linker between those two aromatic centers had a direct influence on the binding affinity of the compounds. In all docked ligands, the phenyl position was unchanged but ligands with shorter linkers (**A11, A12**) or longer (**A14**) imposed changes in the position of the thiazole ring which consequently weakened the binding to the surrounding aromatic amino acids. Changing the substitution within the thiazole ring from 2,5 position (A series) to 2,4 (B series) also resulted in difficulty of adjustment of this aromatic system into the binding site. Location of the protonated amine in the active site of the enzyme is revealed another interesting point. According to the computational predictions at a pH equal to 8 (pH of the cholinesterase bioassays), the monoprotonated form with a charged nitrogen atom from the linker occurs most commonly (64.16%). The diprotonated form was represented only by 31.36% and the monoprotonated form with the charge at a piperazine cyclic system was only 1.5%. Nevertheless, in docking studies, the monoprotonated form as well as the diprotonated form displayed the same binding pattern. The presence of a second proton on the nitrogen in the piperazine system increased the value of the scoring function due to the formation of the cation–π between this fragment and TRP 279. This may indicate that this fraction is mainly responsible for binding with the enzyme. At physiological pH (pH equal to 7.4), its amount increases to 65.28%, which may also corroborate well with the level of enzyme inhibition by the tested compounds. We compared binding mode of **A13** with the conformation presented by donepezil in 1EVE complex. As expected key interactions like cation–π with PHE 330 or aromatic interaction with TRP 84 were common for both ligands. Additionally,

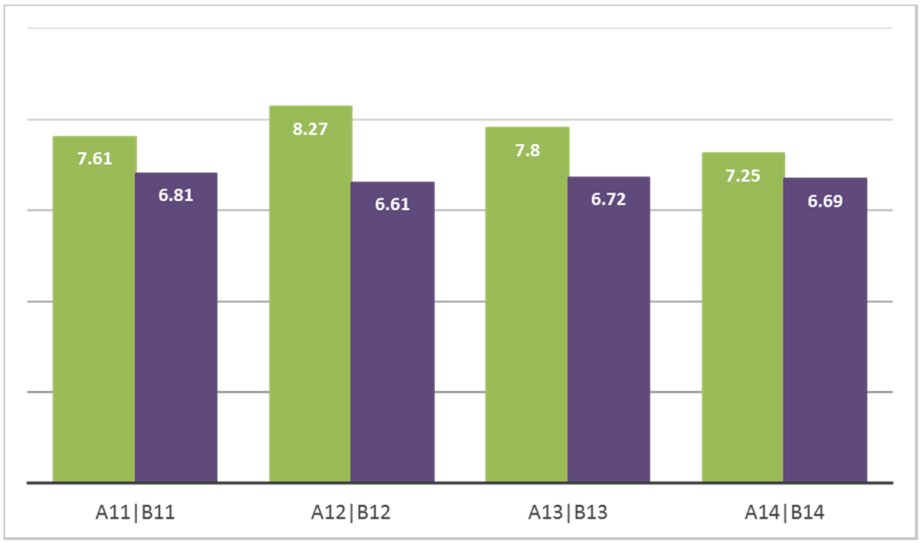

Fig. 4. Comparison of the pA_2 values for selected analogs from series A (green) and B (violet).

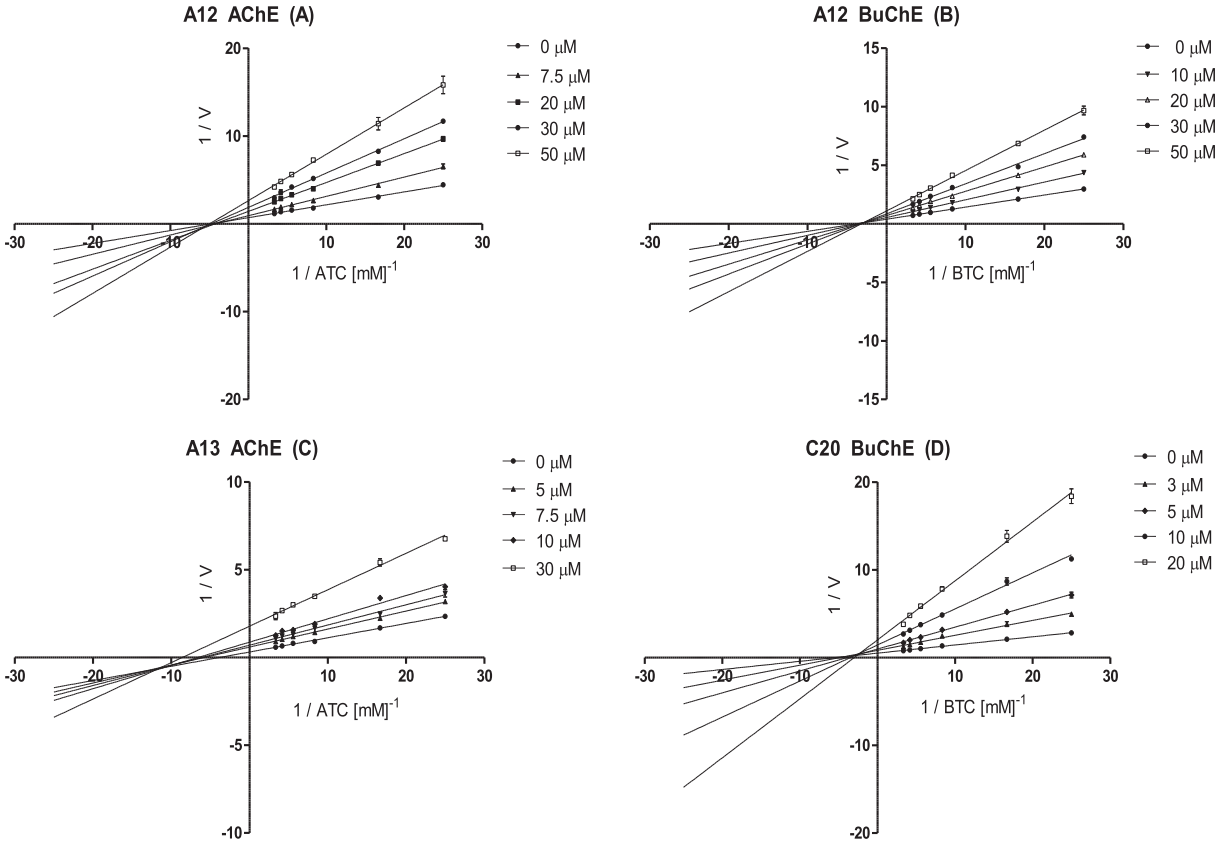

Fig. 5. (A–D). Lineweaver-Burk plots illustrating: mixed types of *ee*AChE inhibition by compounds **A12** (A) and **A13** (C), mixed types of *eq*BuChE inhibition by compounds **A12** (B) and **C20** (D). *V* = initial velocity rate; *ATC* = acetylcholinesterase concentration; *BTC* = butyrylcholinesterase concentration.

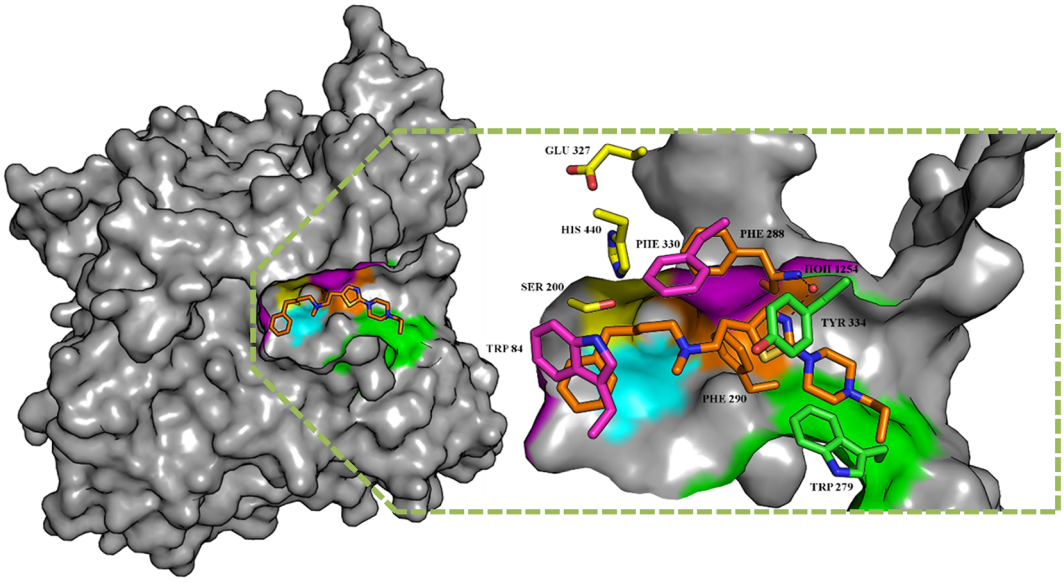

Fig. 6. Binding mode of **A13** (orange) in AChE active site. The colors represent individual parts of the binding site: yellow–catalytic triad, magenta–anion binding site, cyan–oxyanion hole, blue–acyl pocket, green–PAS.

both compounds created hydrogen bond with water molecule HOH 1254 but in case of donepezil oxygen atom from indane-1-one formed a slightly more beneficial bond than that formed by nitrogen atom from thiazole in **A13**. Crucial differences were observed in PAS region. **A13** created aromatic interaction with TYR 334 while donepezil binding was dependent on TRP 279. In case of **A13** TRP 279 participated in cation–π interaction with the second protonated nitrogen but, as already mentioned, only small amount of compound occurred in this form at the pH of the biological assay.

In the case of BuChE, active derivatives were arranged in a large active space—mostly in elongate conformation. As expected, larger, hydrophobic substituents improved both scoring function values and activity. Of the tested compounds, ligand **C20** best illustrates the ligand-protein interaction for BuChE inhibitors (Fig. 7). Among the tested compounds, the strongest inhibitors of BuChE (**C20**, **B14**, **B13** and **C18**) created a CH–π interaction with TRP 231 and a phenyl ring

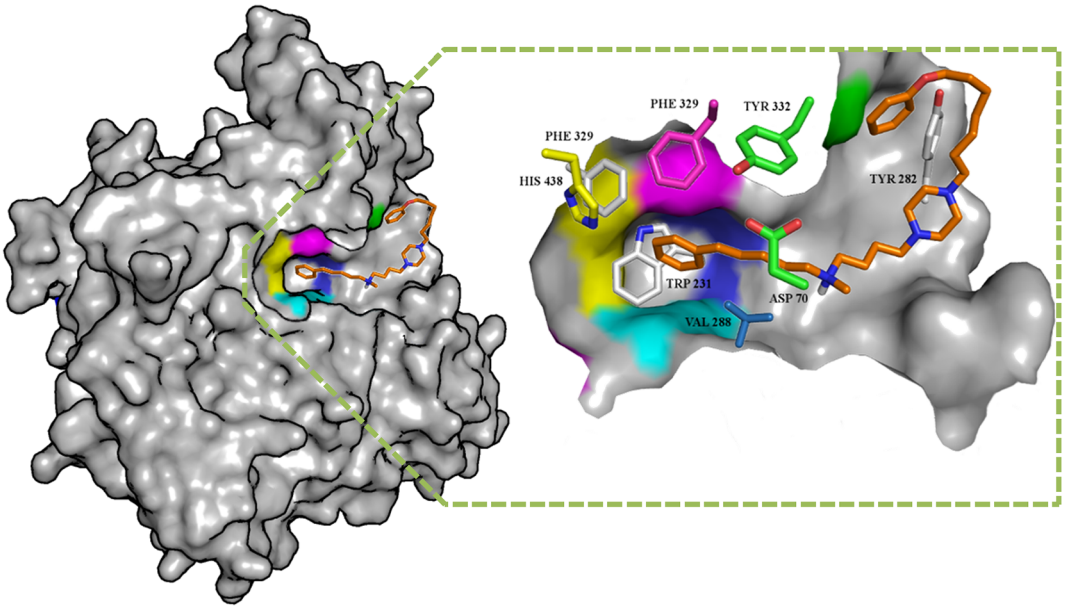

Fig. 7. Position of ligand **C20** (orange) in the active site of the BuChE. The colors represent individual parts of the binding site: yellow–catalytic triad, magenta–anion binding site, cyan–oxyanion hole, blue–acyl pocket, green–PAS.

from phenylalkyl fragment. First, the protonated amine from the linker was situated opposite the entrance to the enzyme active site. Second, the aromatic moiety and piperazine were directed toward TYR 282 and this created a cation–π connection with it. That position of the protonated amine is additionally promoted by ionic interaction with ASP 70. Further, part of the compound is directed toward the entrance to the active site of the enzyme, near the aromatic residue of TYR 332. Docking results indicate that phenoxy fragments do not play a crucial role in the binding mode. Comparison of binding mode of **C20** with tacrine arrangement in crystal structure (PDB: 4BDS) showed how strength of ligand binding depended on specific interactions of the ligand within the active site. Tacrine, smaller and less lipophilic molecule than **C20** was more than thousand times stronger inhibitor of BuChE. High activity of tacrine was caused by its specific interactions with TRP82 and HIS438, additionally stabilized by large net of H-bonds between compound and surrounding water molecules. Larger and more flexible compound **C20** interacted with more amino acids but in a less specific way.

2.3.2. Docking studies on histamine H3 receptor

Using the newly prepared homology model [42], we made an attempt to demonstrate how the tested compounds interacted with the histamine H3 receptor active site. We chose the most active ligand **A12**, to present the observed interactions (Fig. 8). The overall binding mode apparently resembles that described for the known H3 receptor inverse agonist JNJ5207852 [23,42]. Both compounds contain in their structure two nitrogen atoms capable of protonation at physiological pH. The docking results suggest that ionic interaction with GLU 176 (E5.46) in the orthosteric binding site is crucial for efficient binding of non-imidazole H3 antagonists. **A12**, just like JNJ5207852, creates that bond through the nitrogen atom in a heterocyclic system. The thiazole ring is deflected between PHE 163 (F45.55) and TYR 85 (3.33), where aromatic interaction occurs. The distance between PHE 163 (F45.55) and second protonated amine in the ligand aliphatic linker allows the stabilization via cation–π interaction. Further, the phenylpropyl substituent of **A12** was arranged along the part of the allosteric site that is rich in aromatic residues of TM2, TM3 and TM7. Our attempt to explain the differences in the activity between the compounds from series A and B was an important element of the molecular modeling study. The results of biological tests indicated that the pharmacophore common for both series of compounds ensures the ability to reduce the activity of the histamine H3 receptor; however, the substitution of the thiazole at the 2,5-position strengthened this effect. The results obtained during molecular modeling studies suggest that small changes in the geometry of the compound from group B resulting in the disabling of optimal interaction with PHE 163 (F45.55), TYR 344 (6.51), TYR 85 (3.33) and aromatic residues of TM2, TM3 and TM7 are responsible for the activity decline.

2.4. Prediction of physicochemical properties and permeability through the blood-brain barrier

Before the *in vivo* experiments, we carried out studies to predict whether the tested compounds would achieve biological targets located in the central nervous system (CNS), *i.e.*, whether the compounds are capable of penetrating through the blood–brain barrier (BBB). In the first stage, *in silico* experiments were performed. Table 4 shows the values of calculated physicochemical parameters and permeability predictions for four compounds (**A12**, **A13**, **B10** and **C20**) selected for animal testing.

Calculated physicochemical properties for all four compounds were very promising. All tested ligands have a high degree of drug-likeness with particular emphasis on **A12** and **B10** without any violations of the Lipinski rule of 5. Predictions for all tested compounds, with the exception of C20, indicate very good oral absorption, which is particularly important from the point of view of potential therapeutic application. Based on the results of calculations, we can assume that ligands present good (**C20**) or very good (**A12**, **A13**, and **B10**) penetration across the BBB and in commonly used cell systems Caco-2 and MDCK.

2.5. PAMPA assay

In order to confirm the predictions obtained by *in silico* methods, a BBB–PAMPA assay was carried out. Data obtained for the new compounds were compared to standard drugs, where CNS availability is known. Our results (Table 5) clearly demonstrate that compounds labeled as CNS + should be able to cross the BBB by passive diffusion, as their *Pe* values are well above the standard drugs, which are known to be CNS-available (tacrine, donepezile, rivastigmine, chlorpromazine).

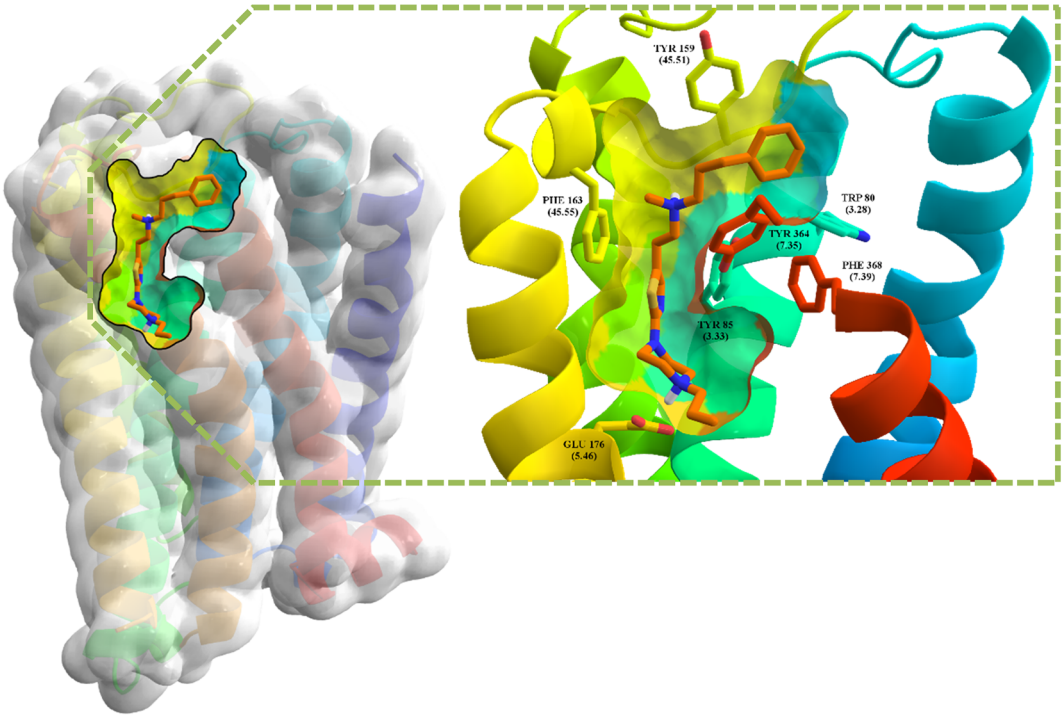

Fig. 8. Binding mode of **A12** (represented by orange sticks) in H3 receptor binding site presents position of ligand (orange) in the active site of the receptor. The colors represent individual transmembrane helices (TMH): blue – TMH1, cyan – TMH2, lime-green – TMH3, green – TMH4, yellow – TMH5, orange – TMH6, red – TMH7.

2.6. *In vivo* study

The aim of the *in vivo* part of this study was to assess the influence of compounds **A12**, **A13**, **B10** and **C20** on fear-motivated contextual memory in the scopolamine model of amnesia in mice. For this purpose, the passive avoidance (PA) task was used. Additionally, to interpret the results obtained in the PA task properly, and to assess the effect of these compounds on animals' general activity and motor coordination, the locomotor activity test and the rotarod test were performed. In the PA task, an overall effect of treatment with the use of scopolamine and compounds **A12, A13, B10** and **C20** was observed ($F[7,132] = 7.509$; $p < 0.0001$). Time also affected the results significantly ($F[1,132] = 54.23$; $p < 0.0001$) and drug × time interaction was significant ($F[7,132] = 8.116$; $p < 0.0001$). Post hoc analysis of the results obtained during the acquisition phase revealed no significant differences in the step-through latencies among experimental groups. In contrast to this, in the retention trial performed on day 2 of PA testing, **A12** at the dose of 30 mg/kg significantly ($p < 0.05$ vs. scopolamine-treated group) prolonged step-through latency. Lower doses of **A12**, as well as compounds **A13, B10** and **C20** at a dose of 30 mg/kg were not active in this task (Fig. 9).

In the locomotor activity test a significant drug effect for **A12** and **A13** was shown ($F[2,105] = 12.75$; $p < 0.0001$). Time did not affect the results significantly ($F[4,105] = 0.5773$; $p > 0.05$) and drug × time interaction was not significant, either ($F[8,105] = 0.7783$; $p > 0.05$). Post hoc analysis revealed a transient but statistically significant decrease of locomotor activity of A12-treated mice only during 12th and 18th min of the test ($p < 0.05$ vs. vehicle; Fig. 10A). Decreased locomotor activity was also noted in **A13**-treated mice between 0 and 6 min ($p < 0.05$) and 12–18 min ($p < 0.001$; Fig. 10A).

Table 4
Selected physicochemical parameters and predictions for penetration by biological structures for multifunctional ligands: **A12**, **A13**, **B10** and **C20** predicted with QikProp.

Principal Descriptors	A12	A13	B10	C20	Range 95% of drugs
Molecular weight	386.597	400.624	358.544	493.774	130.0–725.0
Dipole moment (D)	2.109	2.480	2.141	2.022	1.0–12.5
Molecular volume (A^3)	1380.345	1450.122	1243.305	1840.488	500.0–2000.0
vdW polar surface area (PSA)	23.793	25.094	22.678	21.729	7.0–200.0
No. of rotatable bonds	9.000	10.000	7.000	19.000	0.0–15.0
Donor hydrogen bonds	0.000	0.000	0.000	0.000	0.0–6.0
Acceptor hydrogen bonds	6.000	6.000	6.000	6.750	2.0–20.0
QP log $P_{octanol/water}$	4.419	5.013	3.746	6.868	−2.0 to 6.5
QP log $S_{aqueous\ solubility}$	−3.958	−4.625	−2.695	−5.006	−6.5 to 0.5
QP log $BB_{brain/blood}$	0.644	0.554	0.948	0.170	−3.0 to 1.2
Predicted CNS activity	+ +	+ +	+ +	+	− − to + +
Apparent Caco-2 permeability (nm/*sec*)	390	370	527	142	< 25 poor, > 500 great
Apparent MDCK permeability (nm/*sec*)	295	291	461	81	< 25 poor, > 500 great
Lipinski rule of 5 violations	0	1	0	1	maximum is 4
Jorgensen rule of 3 violations	0	0	0	0	maximum is 3
% Human oral absorption in GI (± 20%)	100	89	100	93	< 25% is poor
Qual. Model for human oral absorption	high	high	high	low	> 80% is high

Table 5
Blood-brain barrier penetration of reference drugs and selected compounds expressed as *Pe* ± SEM (10^{-6} cm/s) (N = 3).

Compound	*Pe* ± SEM (10^{-6} cm/s)	CNS Penetration[a]
A12	9.85 ± 1.2	CNS +
A13	8.2 ± 0.9	CNS +
B10	10.7 ± 1.1	CNS +
C20	9.4 ± 1.9	CNS +
Tacrine	5.3 ± 0.2	CNS +
Donepezil	7.3 ± 0.9	CNS +
Chlorpromazine	5.1 ± 0.3	CNS +
Rivastigmine	6.6 ± 0.5	CNS +
Cefuroxim	2.70 ± 0.1	CNS +/−
Piroxicam	2.20 ± 0.2	CNS +/−
Theophylline	1.1 ± 0.2	CNS −
Atenolol	1.0 ± 0.4	CNS −

[a] CNS (+) (high BBB permeation predicted), Pe (10^{-6} cm/s) > 4.0; CNS (−) (low BBB permeation predicted), Pe (10^{-6} cm/s) ≤ 2.0; CNS (±) (BBB permeation uncertain), 4.0 ≥ Pe (10^{-6} cm/s) > 2.0.

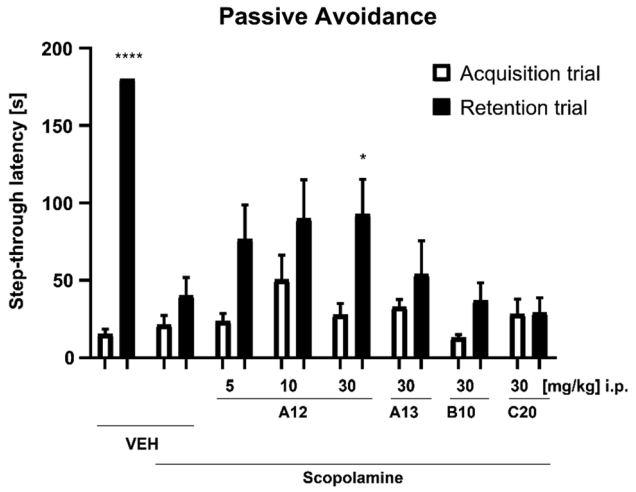

Fig. 9. Influence of the test compounds **A12, A13, B10** and **C20** on fear-motivated memory measured using step-through PA task. Statistical analysis: repeated measures analysis of variance (ANOVA), followed by Sidak's multiple comparison. Significance vs. scopolamine-treated control at the respective trial day: *p < 0.05; **** p < 0.0001.

For **B10** and **C20** an overall effect of treatment was observed ($F[2,95] = 39.33$; $p < 0.0001$). Time did not affect the results significantly ($F[4,95] = 1.726$; $p > 0.05$) and drug × time interaction was not significant, either ($F[8,95] = 1.763$; $p > 0.05$). Post hoc analysis revealed a significant but transient decrease of locomotor activity of **B10**-treated mice only during 18th and 24th min of the test ($p < 0.001$ vs. vehicle; Fig. 10B). Decreased locomotor activity was noted in **C20**-treated mice at each time point of testing: between 0 and 6 min ($p < 0.05$), 6–12 min ($p < 0.01$), 12–24 min ($p < 0.0001$) and 24–30 min ($p < 0.01$) of the test (Fig. 10B).

As shown in Fig. 11, none of the test compounds administered at the dose of 30 mg/kg induced motor deficits in mice at 6 rpm and 18 rpm. Some impairments of motor coordination were observed at 24 rpm, however this effect was not statistically significant ($F[4,35] = 1.00$, $p > 0.05$; Fig. 11C).

3. Conclusion

In the search for new multifunctional compounds as potential anti-Alzheimer's agents, the library of non-imidazole histamine H3 receptor antagonists was investigated. Evaluation of inhibitory potency against eeAChE and eqBuChE made it possible to discover new biological properties of the tested compounds. Twenty-two of the tested compounds showed comparable inhibitory potency for both cholinesterases with IC_{50} values in the micromolar range. Regarding structure-activity-relationship analysis, several conclusions can be drawn. Those compounds with the phenylalkyl substituent connected to an aliphatic amine proved to be stronger inhibitors of both enzymes than their analogs with aliphatic or heterocyclic substituents. Generally, compounds are non-selective inhibitors of both cholinesterases; however, 1-phenoxyalkyl-4-(amino)-alkylpiperazine derivatives (series C) displayed a preference for BuChE. The most potent inhibitor of eeAChE was identified among the thiazol derivatives, **A13** with $IC_{50} = 4.45$ μM, and the most potent inhibitor of eqBuChE was found among the phenoxyalkyl derivatives, **C20** with $IC_{50} = 3.27$ μM.

Results of kinetic studies showed a mixed type of enzyme inhibition which indicates that the test compounds may interact with both catalytic active sites and peripheral anionic sites of cholinesterase at the same time [43]. This has been confirmed by the results of molecular modeling.

Molecular modeling studies have not only revealed possible interactions between the active compounds and their targets but also have shown promising directions for further modifications. Docking results

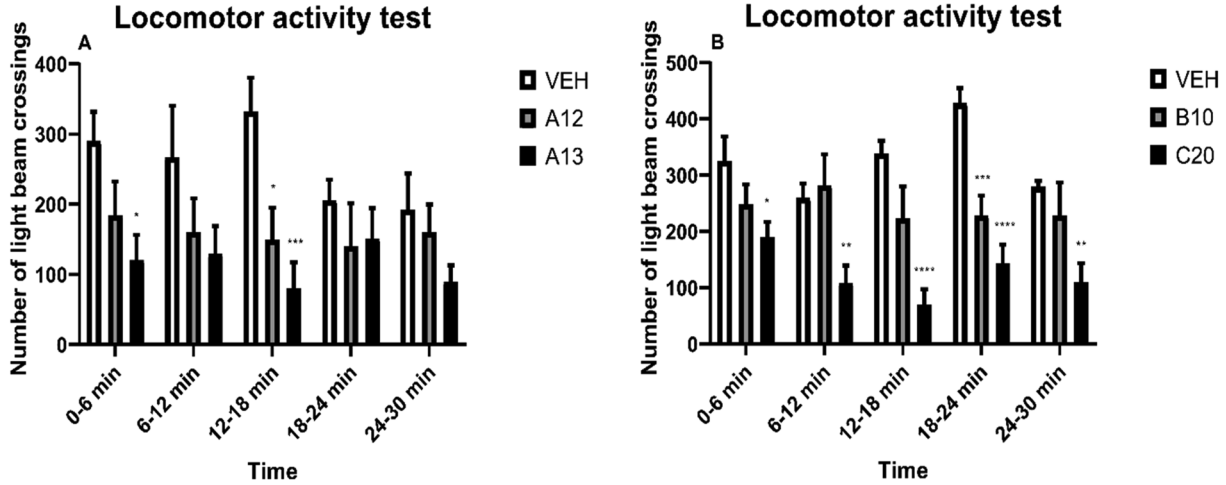

Fig. 10. Influence of the test compounds: **A12**, **A13** (Fig. 10A), **B10** and **C20** (Fig. 10B), each used at 30 mg/kg, on animals' locomotor activity. Statistical analysis: repeated measures ANOVA, followed by Dunnett's post hoc comparison. Significance vs. vehicle-treated mice at the respective time point of testing: * p < 0.05, ** p < 0.01, *** p < 0.001, **** p < 0.0001.

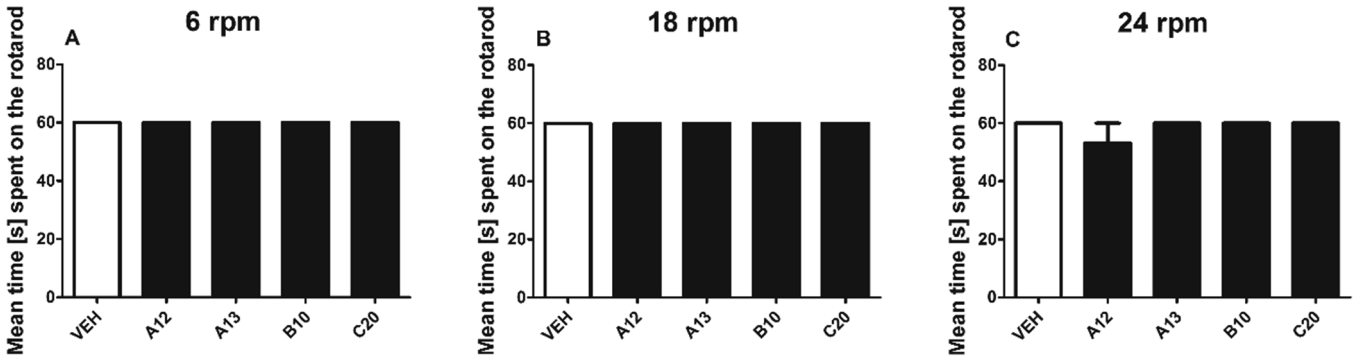

Fig. 11. Influence of the test compounds: **A12, A13, B10** and **C20** tested at the dose of 30 mg/kg on animals' motor coordination measured in the rotarod test at 6 (Fig. 11A), 18 (Fig. 11B) and 24 rpm (Fig. 11C). Statistical analysis: one-way analysis of variance (ANOVA), followed by Dunnett's post hoc test. Results not significant.

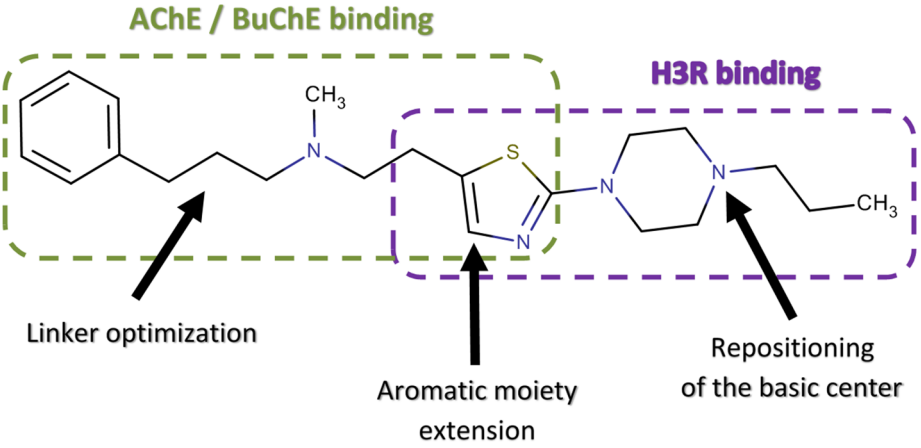

Fig. 12. Proposed modifications of **A12** structure based on results of computational studies.

of the selected compound **A12** allowed us to identify a methyl(3-phenylpropyl)[2-(1,3-thiazol-5-yl)ethyl]amine fragment as responsible for binding to AChE / BuChE and a 1-propyl-4-(1,3-thiazol-2-yl)piperazine fragment responsible for crucial interactions with the H3 receptor. Based on our observations we specified several ways to increase binding strength with selected biological targets (Fig. 12). Development of the aromatic center within thiazole moiety should increase the interactions with both peripheral site of cholinesterases and with the aromatic amino acids in the binding site of the H3 receptor. Improvement in activity can also be achieved by optimizing the distance between aromatic moieties and nitrogen atoms. The proposed changes, apart from improving the activity, are aimed at increasing the drug-likeness of the compounds.

Both, computational studies and *in vitro* assay showed very good physicochemical profiles of compounds for preclinical studies.

In terms of the multi-target profiles of the studied compounds, four of them present interesting *in vitro* properties with various activities toward cholinesterases and histamine H3 receptors. Consequently, we chose compounds **A12** (eeAChE IC_{50} = 13.96 μM, eqBuChE IC_{50} = 14.62 μM and gpH3R pA_2 = 8.27), **A13** (eeAChE IC_{50} = 4.45 μM eqBuChE IC_{50} = 29.62 μM and gpH3R pA_2 = 7.80), **B10** (eeAChE IC_{50} = 18.25 μM, eqBuChE IC_{50} = 23.74 μM and gpH3R pA_2 = 7.12), and **C20** (eeAChE IC_{50} = 13.82 μM, eqBuChE IC_{50} = 15.55 μM and gpH3R pA_2 = 8.27) as good profiling structures to demonstrate which component of a multi-functional compound is the most important to produce a procognitive effect on a mouse. The *in vitro* activity of tested compounds is comparable to the activity of the reference MTDLs (CHEMBL3323053 and CHEMBL380101) which were active during *in vivo* testing.

Performed pharmacological *in vivo* studies revealed anti-amnestic properties of compound **A12** at the dose of 30 mg/kg (i.p.) in the PA task, by applying the mouse model of dementia induced by scopolamine. Moreover, this compound did not affect animals' motor skills, although in an *in vitro* assay its penetration to the CNS was confirmed in the BBB–PAMPA. Compound **A12** is a thiazol derivative and, among the tested compounds, is the most potent histamine H3 receptor antagonist with a moderate anti-cholinergic effect. At this stage of the study, it is difficult to determine whether its anti-amnestic properties *in vivo* depend on the multi-target profile of compound **A12**; however, antagonism of the histamine H3 receptor appears to be an important component. In summary, the obtained results led us to select the most potent multifunctional compound, **A12** with *in vivo* activity, and allow for indication the direction of structural modifications of these multifunctional compounds. Nevertheless the key point of such research will be the maintenance of strong H3 antagonism with improved cholinesterase activity.

4. Methods

4.1. In vitro inhibition of AChE and BuChE

Inhibitory activity of the synthesized compounds against the cholinesterases was measured using the spectrophotometric method described by Ellman et al. modified for 24-well microplates [39]. AChE from electric eel (*ee*AChE) and BuChE from equine serum (*eq*BuChE) were used. 5,5′-Dithiobis-(2-nitrobenzoic acid) (DTNB), acetylthiocholine iodide (ATC), butyrylthiocholine iodide (BTC), and both cholinesterases were purchased from Sigma–Aldrich. The enzymes were

prepared by dissolving 500 U of each in demineralized water to give stock solutions of 5 U/mL. AChE and BuChE were further diluted before use to a final concentration of 1.918 U/mL. In the first step of Ellman's method, 25 μL of the tested compound (or water; i.e., blank samples) was incubated in 0.1 M phosphate buffer (765 μL, pH = 8.0) with the enzyme (20 μL; eeAChE or eqBuChE) at 25 °C. After an incubation period (5 min), 20 μL of DTNB and 20 μL of acetylthiocholine iodide (ATC) or butyrylthiocholine iodide (BTC) solutions (depending on the enzyme used) were added. After another 5 min of incubation, changes in absorbance were measured at 412 nm, using a microplate reader (EnSpire Multimode; PerkinElmer). All the compounds were tested at the screening concentration of 10 μM. The percentage of inhibition was calculated from the equation: $100 - (S/B) \times 100$, where S and B were the enzyme activities with and without the tested compound, respectively. For compounds with inhibitory potency higher than 50%, IC_{50} values were determined. For the IC_{50} measurements, six different concentrations of each compound were used to obtain enzyme activities between 5% and 95%. The IC_{50} values were calculated using nonlinear regression (GraphPad Prism 5. GraphPad Software, San Diego California USA) by plotting the residual enzyme activities against the applied inhibitor concentration. All reactions were performed in triplicate.

4.2. Kinetics studies of AChE and BuChE inhibition

The kinetic studies were performed with compounds **A12**, **A13** and **C20**. We used Ellman's method, modified for 96-well microplates [39]. The aqueous stock solution of eeAChE (5 U/mL) was diluted before use to a final concentration of 0.384 U/mL (0.027 U/mL in the well). The stock solution (0.02125 M) of substrate acetylthiocholine iodide (ATC) was prepared in demineralized water and diluted before use. For each concentration of the test compound, ATC was used at concentrations of 0.3, 0.24, 0.18, 0.12, 0.06, and 0.04 mM in the wells. According to the modified Ellman's protocol, 25 μL of compounds **A12**, **A13** and **C20** (or water; i.e., blank samples) were incubated in 0.1 M phosphate buffer (200 μL, pH = 8.0) with 20 μL of eeAChE and 20 μL of DTNB (0.0025 M; 0.18 mM in the well) at a temperature of 25 °C for 5 min. Six different concentrations of compounds **A12**, **A13** and **C20** were used to obtain enzyme activities between 30% and 80%. After an incubation period, 20 μL of ATC solutions in five concentrations were added. After a further 5 min, the change in absorbance was measured at 412 nm. Each experiment was performed in triplicate. V_{max} and K_m values of the Michaelis-Menten kinetics were calculated by nonlinear regression from substrate-velocity curves. Lineweaver-Burk and Cornish-Bowden plots were calculated using linear regression in GraphPad Prism 5.

4.3. Molecular modeling

4.3.1. Docking procedure

Three-dimensional structures of the ligands were prepared using Corina on-line (Molecular Networks). Sybyl X 1.12 was applied to check the atom types, add hydrogen atoms, and assign Gasteiger-Marsili charges. Protonation and charges were assigned as indicated by predictions obtained with the MarvinSketch 6.2.2 program in accordance with the pH specified for each biological assay conditions. Structures of acetylcholinesterase from the 1EVE crystal structure and butyrylcholinesterase from the 1P0I crystal structure were prepared for docking in the following way: all histidine residues were protonated at Nε, the hydrogen atoms were added, and all ligands were removed. The presence of some water molecules was also taken into account. The binding site of modified 1EVE complex was defined as all amino acid residues within 10 Å of the reference ligand – donepezil. The binding site of the 1P0I complex was defined as all amino acid residues within 20 Å of the butyrate. Docking was performed with GoldSuite 5.3, using a standard set of genetic algorithms with population size 100 and 100,000 operations for each docking pose. As a result, 10 ligand poses, sorted by Chemscore function value, were obtained for each ligand. The results were visualized by PyMOL 0.99rc64.

Algorithms of GOLD docking to both AChE and BuChE were validated in our earlier publication [41]. Docking to AChE was tested by redocking and cross-docking processes with structures from seven crystal complexes with the non-covalently bound inhibitors (1EVE, 1ACJ, 2CKM, 1DX6, 1ACL, 1AX9 and 1VOT). Redocking allowed us to choose the best docking parameters and scoring function. Based on the results of cross-docking AChE complex 1EVE was chosen as the best, multipurpose structure which allowed correct prediction of the conformation of many AChE ligands. RMSD value for the top-scored pose of donepezil obtained during redocking was equal 0.8 Å. In case of butyrylcholinesterase, the docking validation process was slightly different. Due to lack of crystal structures of BuChE with non-covalently bound inhibitors at moment of validation, structure of 1P0I with tacrine was prepared based on AChE complex (PDB: 1ACJ). Further, tacrine was docked into the enzyme from 1P0I and results were compared with binding mode of tacrine from complex prepared by alignment. RMSD for the top-ranked pose was equal 0.9 Å. The same pose compared to the tacrine position, now available in the 4BDS crystal, showed even a better RMSD value equal 0.4 Å.

During the molecular modeling studies on the histamine H3 receptor, a previously prepared homology model was used [42]. Ligand models were prepared in the same way as those used in cholinesterase docking. Docking was performed with Glide from Schrödinger Suite 2017–3 in the standard precision (SP) protocol. The binding site was defined as a box of dimensions 22 × 22 × 22 Å, where the center was identified by the CA atom of Asp 3.32. Ten poses per ligand were collected and analyzed. The best conformation of each ligand obtained during docking was subsequently optimized with Prime in two steps. Primarily, by applying the Monte Carlo method for optimization of ligand and side chains of all amino acids in the receptor model; and subsequently, by applying the same method optimizing ligands with all amino acids (sidechains and backbone) in the receptor model. Obtained results were visualized by PyMOL 0.99rc64.

4.4. Prediction of physicochemical properties and permeability through the brain blood barrier

The *in silico* predictions of physicochemical and pharmacokinetic properties for the test compounds were performed using the QikProp module from Schrödinger Suite 2017–3.

4.5. PAMPA assay

For the prediction of the ability of tested compounds to passively penetrate the BBB, the PAMPA modified protocol was used [44]. Briefly, the filter membrane of the donor plate was coated with PBL (Polar Brain Lipid, Avanti, USA) in dodecane (4 μL of 20 mg/mL PBL in dodecane) and the acceptor well was filled with 300 μL of PBS pH 7.4 buffer (VA). Tested compounds were first dissolved in DMSO and diluted with PBS pH 7.4 to reach the final concentration 100 μM in the donor well. The concentration of DMSO did not exceed 0.5% (V/V) in the donor solution. Next, 300 μL of the donor solution was added to the donor wells (VD) and the donor filter plate was carefully placed on the acceptor plate so that the coated membrane was "in touch" with both donor solution and acceptor buffer. The test compound diffused from the donor well through the lipid membrane (Area = 0.28 cm^2) to the acceptor well. The amount of the drug (n) in both donor and the acceptor wells was assessed after 3, 4, 5 and 6 h of incubation in quadruplicate using a Synergy HT UV plate reader (Biotek, USA) at the maximum absorption wavelength of each compound. The concentration of the compounds was calculated from the standard curve and expressed as the permeability (Pe) according the equation:

$$Pe = \mathrm{C} \times -\ln\left(\frac{1 - n_{acceptor}}{n_{total}}\right) \text{ where } C = \left(\frac{V_D \times V_A}{(V_D \times V_A) \times Area \times time}\right)$$

4.6. In vivo experiments

4.6.1. Animals and housing conditions

Adult male Albino Swiss (CD-1) mice weighing 18–22 g were used in behavioral tests. The animals were housed in groups of 10 mice per cage at a room temperature of 22 ± 2 °C, under a light/dark (12:12) cycle. The animals had free access to food and water before experiments. The ambient temperature of the room and the humidity were kept consistent throughout all the tests. For the experiments, the animals were selected randomly. Each experimental group consisted of 8–10 animals/dose and each mouse was used only once. The experiments were performed between 8 AM and 2 PM. Immediately after *in vivo* assays, the animals were euthanized by cervical dislocation. All procedures were approved by the Local Ethics Committee of the Jagiellonian University in Kraków and the treatment of animals was in full accordance with ethical standards laid down in respective Polish and EU regulations (Directive No. 86/609/EEC).

4.6.2. Chemicals used in the in vivo tests

The test compounds were synthesized at the Department of Synthesis and Technology of Drugs, Medical University of Łódź. For *in vivo* studies, they were suspended in 1% Tween 80 (Polskie Odczynniki Chemiczne, Poland) and administered intraperitoneally (*i.p.*) 60 min before the test. Control mice were given an appropriate amount of vehicle (1% Tween 80). (-)-Scopolamine hydrobromide was purchased from Sigma–Aldrich (Poland). To induce memory impairments, it was dissolved in 0.9% saline solution and administered *i.p.* at a dose of 1 mg/kg 30 min before the acquisition trial of the PA task.

4.6.3. Behavioral testing protocol

4.6.3.1. PA task (fear-motivated contextual memory task). The influence of the test compounds on acquisition and retention of the PA task was conducted as previously described by Park et al. [45]. For this purpose, the PA apparatus (Panlab Harvard Apparatus, Spain) was used. This consists of a large white-painted illuminated compartment (26 × 26 × 34 cm) and a small black-painted dark compartment (13 × 7.5 × 7.5 cm) separated from each other by a guillotine gate. To assess the effect of the test compound on scopolamine-induced memory impairments, the animals underwent two separate trials: an acquisition trial (conditioning phase) and a retention trial (testing phase). The latter was conducted 24 h after the acquisition trial.

For the acquisition trial, the mouse was initially placed for 30 s in the light compartment (exploration period; guillotine gate is closed). At the end of the exploration period, the guillotine door (5 × 5 cm) between the light and the dark compartments was opened and the time elapsed before entering the black chamber was recorded. As soon as the mouse entered the dark compartment, the door automatically closed and an electrical shock (current intensity: 0.2 mA, duration: 2 s) was delivered through the grid floor.

For the retention trial, the mice were placed in the illuminated, white compartment again and the latency time between door opening and entry into the dark compartment was recorded for each mouse. If the mouse did not enter the dark compartment within 180 s (cut off latency), it was concluded that it remembered the foot shock from the acquisition trial. Better memory performance was indicated by longer latency to enter the black chamber in the test (retention) phase than in the conditioning (acquisition) phase.

4.6.3.2. Locomotor activity test. The locomotor activity test was performed using activity cages (40 × 40 × 31 cm, supplied with I.R. beam emitters) (Activity Cage 7441, Ugo Basile, Italy) connected to a counter for the recording of light-beam interruptions. Sixty minutes before the experiment, the mice were *i.p.* pretreated with the tested compound or the vehicle (1% Tween 80), and then individually placed in the activity cages in a sound-attenuated room. The animals' movements (*i.e.*, the number of light-beam crossings) were counted during the next 30 min at five 6-min each intervals [46].

4.6.3.3. Rotarod test. The test was performed according to the method recently described by Sałat et al. [47]. Briefly, the mice were trained daily for 3 days on the rotarod apparatus (Rotarod apparatus, May Commat RR0711, Turkey; rod diameter: 2 cm), rotating at a constant speed of 18 rotations per minute (rpm). During each training session, the animals were placed on a rotating rod for 3 min with an unlimited number of trials. The experimentation proper was conducted at least 24 h after the final training trial. On the test day, 60 min before the rotarod test, the mice were *i.p.* pretreated with the test compound or the vehicle. Then, the animals were tested on the rotarod apparatus revolving at 6, 18, 24 rpm. Motor impairments, defined as the inability to remain on the rod for 1 min, were measured at each speed and the mean time spent on the rotating rod was counted.

4.6.4. Data analysis

Data analysis of the *in vivo* results was provided by GraphPad Prism Software (v.8, CA, USA). Numerical results from the tests are expressed as mean ± SEM. The results were statistically evaluated using one-way analysis of variance (ANOVA), followed by Dunnett's post hoc comparison or two-way repeated measures ANOVA, followed by Sidak's or Dunnett's multiple comparisons. $P < 0.05$ was considered significant.

Declaration of Competing Interest

There are no conflicts of interest.

Acknowledgements

Financial support in the form of a research grant (UMO-2014/15/N/NZ7/02965) from the National Science Center in Poland, the Jagiellonian University Medical College grant K/ZDS/007213, the European Cooperation in Science and Technology COST Action CA15135, European Regional Development Fund: Project "PharmaBrain" (no. CZ.02.1.01/0.0/0.0/16_025/0007444) and support from MH CZ—DRO (UHHK, 00179906) is gratefully acknowledged. Study was also sponsored by Polpharma Scientific Foundation.

Appendix A. Supplementary material

Supplementary data to this article can be found online at https://doi.org/10.1016/j.bioorg.2019.103084.

References

[1] S.F. Cappa, The quest for an Alzheimer therapy, Front. Neurol. 9 (2018) 108, https://doi.org/10.3389/fneur.2018.00108.
[2] B. Winblad, P. Amouyel, S. Andrieu, C. Ballard, C. Brayne, H. Brodaty, A. Cedazo-Minguez, B. Dubois, D. Edvardsson, H. Feldman, L. Fratiglioni, G.B. Frisoni, S. Gauthier, J. Georges, C. Graff, K. Iqbal, F. Jessen, G. Johansson, L. Jönsson, M. Kivipelto, M. Knapp, F. Mangialasche, R. Melis, A. Nordberg, M.O. Rikkert, C. Qiu, T.P. Sakmar, P. Scheltens, L.S. Schneider, R. Sperling, L.O. Tjernberg, G. Waldemar, A. Wimo, H. Zetterberg, Defeating Alzheimer's disease and other dementias: a priority for European science and society, Lancet Neurol. 15 (2016) 455–532, https://doi.org/10.1016/S1474-4422(16)00062-4.
[3] R. Morphy, Z. Rankovic, Designing multiple ligands – medicinal chemistry strategies and challenges, Curr. Pharm. Des. 15 (2009) 587–600, https://doi.org/10.2174/138161209787315594.
[4] A. Talevi, Multi-target pharmacology: possibilities and limitations of the "skeleton key approach" from a medicinal chemist perspective, Front. Pharmacol. 6 (2015) 205, https://doi.org/10.3389/fphar.2015.00205.
[5] M. Rosini, E. Simoni, R. Caporaso, A. Minarini, Multitarget strategies in Alzheimer's disease: benefits and challenges on the road to therapeutics, Future Med. Chem. 8 (2016) 697–711, https://doi.org/10.4155/fmc-2016-0003.
[6] R. León, A.G. Garcia, J. Marco-Contelles, Recent advances in the multitarget-

directed ligands approach for the treatment of Alzheimer's disease, Med. Res. Rev. 33 (2013) 139–189, https://doi.org/10.1002/med.20248.
[7] K.S.T. Dias, C. Viegas, Multi-target directed drugs: a modern approach for design of new drugs for the treatment of Alzheimer's disease, Curr. Neuropharmacol. 12 (2014) 239–255, https://doi.org/10.2174/1570159X1203140511153200.
[8] F. Prati, A. Cavalli, M.L. Bolognesi, Navigating the chemical space of multitarget-directed ligands: from hybrids to fragments in Alzheimer's disease, Molecules 21 (2016) 466, https://doi.org/10.3390/molecules21040466.
[9] B. Sadek, N. Khan, F.H. Darras, S. Pockes, M. Decker, The dual-acting AChE inhibitor and H3 receptor antagonist UW-MD-72 reverses amnesia induced by scopolamine or dizocilpine in passive avoidance paradigm in rats, Physiol. Behav. 165 (2016) 383–391, https://doi.org/10.1016/J.PHYSBEH.2016.08.022.
[10] B. Sadek, A. Saad, A. Sadeq, F. Jalal, H. Stark, Histamine H3 receptor as a potential target for cognitive symptoms in neuropsychiatric diseases, Behav. Brain Res. 312 (2016) 415–430, https://doi.org/10.1016/j.bbr.2016.06.051.
[11] P.T. Francis, A.M. Palmer, M. Snape, G.K. Wilcock, The cholinergic hypothesis of Alzheimer's disease: a review of progress (accessed July 9, 2018), J. Neurol. Neurosurg. Psyc. 66 (1999) 137–147 http://www.ncbi.nlm.nih.gov/pubmed/10071091.
[12] F. Zemek, L. Drtinova, E. Nepovimova, V. Sepsova, J. Korabecny, J. Klimes, K. Kuca, Outcomes of Alzheimer's disease therapy with acetylcholinesterase inhibitors and memantine, Exp. Opin. Drug Saf. 13 (2014) 759–774, https://doi.org/10.1517/14740338.2014.914168.
[13] M. Bond, G. Rogers, J. Peters, R. Anderson, M. Hoyle, A. Miners, T. Moxham, S. Davis, P. Thokala, A. Wailoo, M. Jeffreys, C. Hyde, The effectiveness and cost-effectiveness of donepezil, galantamine, rivastigmine and memantine for the treatment of Alzheimer's disease (review of Technology Appraisal No. 111): a systematic review and economic model, Health Technol. Assess. (Rockv). 16 (2012) 1–470, https://doi.org/10.3310/hta16210.
[14] M. Bajda, K. Łątka, M. Hebda, J. Jończyk, B. Malawska, Novel carbamate derivatives as selective butyrylcholinesterase inhibitors, Bioorg. Chem. 78 (2018) 29–38, https://doi.org/10.1016/j.bioorg.2018.03.003.
[15] J. Wiemann, A. Loesche, R. Csuk, Novel dehydroabietylamine derivatives as potent inhibitors of acetylcholinesterase, Bioorg. Chem. 74 (2017) 145–157, https://doi.org/10.1016/j.bioorg.2017.07.013.
[16] T. Mochizuki, K. Okakura-Mochizuki, A. Horii, Y. Yamamoto, A. Yamatodani, Histaminergic modulation of hippocampal acetylcholine release in vivo, J. Neurochem. 62 (2008) 2275–2282, https://doi.org/10.1046/j.1471-4159.1994.62062275.x.
[17] S. Bertoni, V. Ballabeni, L. Flammini, F. Saccani, G. Domenichini, G. Morini, M. Comini, M. Rivara, E. Barocelli, In vitro and in vivo pharmacological analysis of imidazole-free histamine H3 receptor antagonists: promising results for a brain-penetrating H3 blocker with weak anticholinesterase activity, Naunyn. Schmiedebergs. Arch. Pharmacol. 378 (2008) 335–343, https://doi.org/10.1007/s00210-008-0299-2.
[18] R. Grove, C. Harrington, A. Mahler, I. Beresford, P. Maruff, M. Lowy, A. Nicholls, R. Boardley, A. Berges, P. Nathan, J. Horrigan, A. Randomized, Double-blind, placebo-controlled, 16-week study of the H3 receptor antagonist, GSK239512 as a monotherapy in subjects with mild-to-moderate Alzheimer's disease, Curr. Alzheimer Res. 11 (2014) 47–58, https://doi.org/10.2174/1567205010666131212110148.
[19] W. Cho, P. Maruff, J. Connell, C. Gargano, N. Calder, S. Doran, S. Fox-Bosetti, A. Hassan, J. Renger, G. Herman, C. Lines, A. Verma, Additive effects of a cholinesterase inhibitor and a histamine inverse agonist on scopolamine deficits in humans, Psychopharmacology 218 (2011) 513–524, https://doi.org/10.1007/s00213-011-2344-y.
[20] J.-C. Schwartz, The histamine H3 receptor: from discovery to clinical trials with pitolisant, Br. J. Pharmacol. 163 (2011) 713–721, https://doi.org/10.1111/j.1476-5381.2011.01286.x.
[21] R. Guryn, M. Staszewski, K. Walczyński, Non-imidazole histamine H3 ligands: part V. synthesis and preliminary pharmacological investigation of 1-[2-thiazol-4-yl- and 1-[2-thiazol-5-yl-(2-aminoethyl)]-4-n-propylpiperazine derivatives, Med. Chem. Res. 22 (2013) 3640–3652, https://doi.org/10.1007/s00044-012-0372-8.
[22] S. Liedtke, K. Flau, M. Kathmann, E. Schlicker, H. Stark, G. Meier, W. Schunack, Replacement of imidazole by a piperidine moiety differentially affects the potency of histamine H3-receptor antagonists, Naunyn. Schmiedebergs. Arch. Pharmacol. 367 (2003) 43–50, https://doi.org/10.1007/s00210-002-0649-4.
[23] A.J. Barbier, C. Berridge, C. Dugovic, A.D. Laposky, S.J. Wilson, J. Boggs, L. Aluisio, B. Lord, C. Mazur, C.M. Pudiak, X. Langlois, W. Xiao, R. Apodaca, N.I. Carruthers, T.W. Lovenberg, Acute wake-promoting actions of JNJ-5207852, a novel, diamine-based H3 antagonist, Br. J. Pharmacol. 143 (2004) 649–661, https://doi.org/10.1038/sj.bjp.0705964.
[24] N. Khan, A. Saad, S.M. Nurulain, F.H. Darras, M. Decker, B. Sadek, The dual-acting H3 receptor antagonist and AChE inhibitor UW-MD-71 dose-dependently enhances memory retrieval and reverses dizocilpine-induced memory impairment in rats, Behav. Brain Res. 297 (2016) 155–164, https://doi.org/10.1016/j.bbr.2015.10.022.
[25] K. Kuder, D. Łażewska, G. Latacz, J.S. Schwed, T. Karcz, H. Stark, J. Karolak-Wojciechowska, K. Kieć-Kononowicz, Chlorophenoxy aminoalkyl derivatives as histamine H3R ligands and antiseizure agents, Bioorg. Med. Chem. 24 (2016) 53–72, https://doi.org/10.1016/J.BMC.2015.11.021.
[26] W. Huang, L. Tang, Y. Shi, S. Huang, L. Xu, R. Sheng, P. Wu, J. Li, N. Zhou, Y. Hu, Searching for the multi-target-directed ligands against Alzheimer's disease: discovery of quinoxaline-based hybrid compounds with AChE, H3R and BACE 1 inhibitory activities, Bioorg. Med. Chem. 19 (2011) 7158–7167, https://doi.org/10.1016/J.BMC.2011.09.061.
[27] D. Łażewska, J. Jończyk, M. Bajda, N. Szałaj, A. Więckowska, D. Panek, C. Moore, K. Kuder, B. Malawska, K. Kieć-Kononowicz, Cholinesterase inhibitory activity of chlorophenoxy derivatives - histamine H3receptor ligands, Bioorgan. Med. Chem. Lett. 26 (2016) 4140–4145, https://doi.org/10.1016/j.bmcl.2016.04.054.
[28] J. Fang, Y. Li, R. Liu, X. Pang, C. Li, R. Yang, Y. He, W. Lian, A.L. Liu, G.H. Du, Discovery of multitarget-directed ligands against Alzheimer's disease through systematic prediction of chemical-protein interactions, J. Chem. Inf. Model. 55 (2015) 149–164, https://doi.org/10.1021/ci500574n.
[29] G. Petroianu, K. Arafat, B.C. Sasse, H. Stark, Multiple enzyme inhibitions by histamine H3 receptor antagonists as potential procognitive agents, Pharmazie 61 (2006) 179–182 (accessed February 4, 2019), https://www.ingentaconnect.com/content/govi/pharmaz/2006/00000061/00000003/art00003.
[30] S. Kumar, S. Chowdhury, S. Kumar, In silico repurposing of antipsychotic drugs for Alzheimer's disease, BMC Neurosci. 18 (2017) 76, https://doi.org/10.1186/s12868-017-0394-8.
[31] M. Shoaib, M.A. Kamal, S.M. Danish Rizvi, Repurposed drugs as potential therapeutic candidates for the management of Alzheimer's disease, Curr. Drug Metab. 18 (2017) 842–852, https://doi.org/10.2174/1389200218666170607101622.
[32] X. Wang, S. Chong, H. Lin, Z. Yan, F. Huang, Z. Zeng, X. Zhang, Y. Su, Discovery of atorvastatin as a tetramer stabilizer of nuclear receptor RXRα through structure-based virtual screening, Bioorg. Chem. 85 (2019) 413–419, https://doi.org/10.1016/j.bioorg.2019.01.007.
[33] D. Panek, A. Więckowska, J. Jończyk, J. Godyń, M. Bajda, T. Wichur, A. Pasieka, D. Knez, A. Pišlar, J. Korabecny, O. Soukup, V. Sepsova, R. Sabaté, J. Kos, S. Gobec, B. Malawska, Design, synthesis, and biological evaluation of 1-benzylamino-2-hydroxyalkyl derivatives as new potential disease-modifying multifunctional anti-Alzheimer's agents, ACS Chem. Neurosci. 9 (2018) 1074–1094, https://doi.org/10.1021/acschemneuro.7b00461.
[34] N. Guzior, M. Bajda, J. Rakoczy, B. Brus, S. Gobec, B. Malawska, Isoindoline-1,3-dione derivatives targeting cholinesterases: design, synthesis and biological evaluation of potential anti-Alzheimer's agents, Bioorg. Med. Chem. 23 (2015) 1629–1637, https://doi.org/10.1016/j.bmc.2015.01.045.
[35] K. Czarnecka, P. Szymański, M. Girek, E. Mikiciuk-Olasik, R. Skibiński, J. Kabziński, I. Majsterek, B. Malawska, J. Jończyk, M. Bajda, Tetrahydroacridine derivatives with fluorobenzoic acid moiety as multifunctional agents for Alzheimer's disease treatment, Bioorg. Chem. 72 (2017) 315–322, https://doi.org/10.1016/j.bioorg.2017.05.003.
[36] A. Frymarkiewicz, K. Walczyński, Non-imidazole histamine H3 ligands, Part IV: SAR of 1-[2-thiazol-5-yl-(2-aminoethyl)]-4-n-propylpiperazine derivatives, Eur. J. Med. Chem. 44 (2009) 1674–1681, https://doi.org/10.1016/j.ejmech.2008.09.019.
[37] R. Guryn, M. Staszewski, P. Kopczacki, K. Walczyński, Non-imidazole histamine H3 ligands. Part VI. Synthesis and preliminary pharmacological investigation of thiazole-type histamine H3-receptor antagonists with lacking a nitrogen nucleus in the side chain, Med. Chem. (2016) (accessed March 7, 2017), http://www.ncbi.nlm.nih.gov/pubmed/27220560.
[38] M. Staszewski, K. Walczyński, 1-Phenoxyalkyl-4-[(N, N-disubstitutedamino)alkyl] piperazine derivatives as non-imidazole histamine H3-antagonists, Med. Chem. Res. 22 (2013) 1287–1304, https://doi.org/10.1007/s00044-012-0090-2.
[39] G.L. Ellman, K.D. Courtney, V. Andres, R.M. Featherstone, A new and rapid colorimetric determination of acetylcholinesterase activity, Biochem. Pharmacol. 7 (1961) 88–95, https://doi.org/10.1016/0006-2952(61)90145-9.
[40] R.B. Silverman, The organic chemistry of enzyme-catalyzed reactions, Academic Press, 2002.
[41] M. Bajda, A. Więckowska, M. Hebda, N. Guzior, C. Sotriffer, B. Malawska, Structure-based search for new inhibitors of cholinesterases, Int. J. Mol. Sci. 14 (2013) 5608–5632, https://doi.org/10.3390/ijms14035608.
[42] J. Jończyk, B. Malawska, M. Bajda, Hybrid approach to structure modeling of the histamine H3 receptor: multi-level assessment as a tool for model verification, PLoS ONE 12 (2017) e0186108, https://doi.org/10.1371/journal.pone.0186108.
[43] R. Caliandro, A. Pesaresi, L. Cariati, A. Procopio, M. Oliverio, D. Lamba, Kinetic and structural studies on the interactions of Torpedo californica acetylcholinesterase with two donepezil-like rigid analogues, J. Enzyme Inhib. Med. Chem. 33 (2018) 794–803, https://doi.org/10.1080/14756366.2018.1458030.
[44] L. Di, E.H. Kerns, K. Fan, O.J. McConnell, G.T. Carter, High throughput artificial membrane permeability assay for blood-brain barrier, Eur. J. Med. Chem. 38 (2003) 223–232 (accessed July 10, 2018), http://www.ncbi.nlm.nih.gov/pubmed/12667689.
[45] S.J. Park, D.H. Kim, J.M. Jung, J.M. Kim, M. Cai, X. Liu, J.G. Hong, C.H. Lee, K.R. Lee, J.H. Ryu, The ameliorating effects of stigmasterol on scopolamine-induced memory impairments in mice, Eur. J. Med. Chem. 676 (1–3) (2012) 64–70, https://doi.org/10.1016/j.ejphar.2011.11.050.
[46] K. Sałat, K. Kulig, J. Gajda, K. Więckowski, B. Filipek, B. Malawska, Evaluation of anxiolytic-like, anticonvulsant, antidepressant-like and antinociceptive properties of new 2-substituted 4-hydroxybutanamides with affinity for GABA transporters in mice, Pharmacol. Biochem. Behav. 110 (2013) 145–153, https://doi.org/10.1016/j.pbb.2013.06.013.
[47] K. Salat, T. Librowski, A. Moniczewski, K. Stanisz-Wallis, K. Wieckowski, B. Malawska, Analgesic, antioedematous and antioxidant activity of γ-butyrolactone derivatives in rodents, Behav. Pharmacol. 23 (2012) 407–416, https://doi.org/10.1097/FBP.0b013e3283566042.